

Using automated vegetation cover estimation from close-range photogrammetric point clouds to compare vegetation location properties in mountain terrain

R. Niederheiser , M. Winkler , V. Di Cecco , B. Erschbamer , R. Fernández , C. Geitner , Hannah Hofbauer , C. Kalaitzidis , Barbara Klingraber , A. Lamprecht , J. Lorite , L. Nicklas , P. Nyktas , H. Pauli , A. Stanisci , K. Steinbauer , J.-P. Theurillat , P. Vittoz & M. Rutzinger

To cite this article: R. Niederheiser , M. Winkler , V. Di Cecco , B. Erschbamer , R. Fernández , C. Geitner , Hannah Hofbauer , C. Kalaitzidis , Barbara Klingraber , A. Lamprecht , J. Lorite , L. Nicklas , P. Nyktas , H. Pauli , A. Stanisci , K. Steinbauer , J.-P. Theurillat , P. Vittoz & M. Rutzinger (2021): Using automated vegetation cover estimation from close-range photogrammetric point clouds to compare vegetation location properties in mountain terrain, GIScience & Remote Sensing, DOI: [10.1080/15481603.2020.1859264](https://doi.org/10.1080/15481603.2020.1859264)

To link to this article: <https://doi.org/10.1080/15481603.2020.1859264>



© 2021 The Author(s). Published by Informa UK Limited, trading as Taylor & Francis Group.



[View supplementary material](#)



Published online: 13 Jan 2021.



[Submit your article to this journal](#)



Article views: 256














[View related articles](#)



[View Crossmark data](#)

Using automated vegetation cover estimation from close-range photogrammetric point clouds to compare vegetation location properties in mountain terrain

R. Niederheiser ^a, M. Winkler ^b, V. Di Cecco^c, B. Erschbamer^d, R. Fernández^e, C. Geitner^a, Hannah Hofbauer^b, C. Kalaitzidis^f, Barbara Klingraber^b, A. Lamprecht ^g, J. Lorite^e, L. Nicklas ^d, P. Nyktas ^g, H. Pauli ^b, A. Stanisci ^h, K. Steinbauer ^b, J.-P. Theurillat ^{ij}, P. Vittoz ^k and M. Rutzinger ^{a,j}

^aInstitute of Geography, University of Innsbruck, Innsbruck, Austria; ^bGLORIA Coordination, Department of Integrative Biology and Biodiversity Research, University of Natural Resources and Life Sciences (BOKU), Vienna & Institute for Interdisciplinary Mountain Research, Austrian Academy of Sciences, Vienna, Austria; ^cMajella Seed Bank, Lama Dei Peligni, Italy; ^dDepartment of Botany, University of Innsbruck, Innsbruck, Austria; ^eDepartment of Botany, University of Granada, Granada, Spain; ^fDepartment of Geo-information in Environmental Management, Mediterranean Agronomic Institute of Chania, Chania, Greece; ^gDepartment of Natural Resources, Faculty of Geo-Information Science and Earth Observation, University of Twente, Enschede, Netherlands; ^hDep. Bioscience and Territory, University of Molise, Termoli, Italy; ⁱCentre Alpien De Phytogéographie, Fondation J.-M. Aubert, Champex-Lac, Switzerland; ^jDepartment of Botany and Plant Biology, Section of Biology, University of Geneva, Chambésy, Switzerland; ^kInstitute of Earth Surface Dynamics, Faculty of Geosciences and Environment, University of Lausanne, Lausanne, Switzerland; ^lInstitute for Interdisciplinary Mountain Research, Austrian Academy of Sciences, Innsbruck, Austria

ABSTRACT

In this paper we present a low-cost approach to mapping vegetation cover by means of high-resolution close-range terrestrial photogrammetry. A total of 249 clusters of nine 1 m² plots each, arranged in a 3 × 3 grid, were set up on 18 summits in Mediterranean mountain regions and in the Alps to capture images for photogrammetric processing and *in-situ* vegetation cover estimates. This was done with a hand-held pole-mounted digital single-lens reflex (DSLR) camera. Low-growing vegetation was automatically segmented using high-resolution point clouds. For classifying vegetation we used a two-step semi-supervised Random Forest approach. First, we applied an expert-based rule set using the Excess Green index (ExG) to predefine non-vegetation and vegetation points. Second, we applied a Random Forest classifier to further enhance the classification of vegetation points using selected topographic parameters (elevation, slope, aspect, roughness, potential solar irradiation) and additional vegetation indices (Excess Green Minus Excess Red (ExGR) and the vegetation index VEG). For ground cover estimation the photogrammetric point clouds were meshed using Screened Poisson Reconstruction. The relative influence of the topographic parameters on the vegetation cover was determined with linear mixed-effects models (LMMs). Analysis of the LMMs revealed a high impact of elevation, aspect, solar irradiation, and standard deviation of slope. The presented approach goes beyond vegetation cover values based on conventional orthoimages and *in-situ* vegetation cover estimates from field surveys in that it is able to differentiate complete 3D surface areas, including overhangs, and can distinguish between vegetation-covered and other surfaces in an automated manner. The results of the Random Forest classification confirmed it as suitable for vegetation classification, but the relative feature importance values indicate that the classifier did not leverage the potential of the included topographic parameters. In contrast, our application of LMMs utilized the topographic parameters and was able to reveal dependencies in the two biomes, such as elevation and aspect, which were able to explain between 87% and 92.5% of variance.

ARTICLE HISTORY

Received 8 April 2020
Accepted 27 November 2020

KEYWORDS

High-mountain vegetation; vegetation stand properties; topographic parameters; 3D point cloud processing; random forest; linear mixed-effects model

1. Introduction

In the absence of shading by shrubs and trees, habitat conditions at high elevations are heavily influenced by topography, which affects the increasing incident solar radiation on bright days, and by wind exposure (Winkler et al. 2016). On the micro-scale, the rugged alpine terrain varies greatly in temperature, especially

over very short distances, and in hydrological conditions (Körner 2003). A precise mapping of topography in conjunction with vegetation cover may help to better understand the importance of the pattern of habitats, their effect on the thermal regimes experienced by plant species at high elevations, and may complement the research of botany experts to better characterize vegetation locations (Zellweger et al.

CONTACT Martin Rutzinger  martin.rutzinger@uibk.ac.at

 Supplemental data for this article can be accessed [here](#)

© 2021 The Author(s). Published by Informa UK Limited, trading as Taylor & Francis Group.

This is an Open Access article distributed under the terms of the Creative Commons Attribution-NonCommercial-NoDerivatives License (<http://creativecommons.org/licenses/by-nc-nd/4.0/>), which permits non-commercial re-use, distribution, and reproduction in any medium, provided the original work is properly cited, and is not altered, transformed, or built upon in any way.

2019). Also, a more detailed knowledge of the influence of micro-topography on micro-habitats may help in improving species distribution models.

A standard manual field sampling procedure to quantitatively assess vegetation cover at plot level is visual cover estimation, followed by pointing with a grid frame, e.g. for species frequency studies. Vegetation cover is assessed by perpendicularly lowering a sampling pin at regularly distributed grid points and counting intersections with vegetation (Friedmann et al. 2011; Pauli et al. 2015). When mapping vegetation in remotely sensed imagery, spatial resolution is a key criterion for mapping in spatially heterogeneous landscapes in addition to topographic data (Räsänen and Virtanen 2019). The image resolution of airborne and satellite-based imagery makes them suitable for regional studies, but has only been used in few cases for alpine mountain-top vegetation (Mohapatra et al. 2019; Wakulińska and Marcinkowska-Ochtyra 2020; Zhang, Yao, and Suo 2020). Recent vegetation mapping approaches using remotely sensed imagery by unmanned aerial vehicle (UAV) combined with object-based image analysis have been successful (Lucieer et al. 2014; Wallace et al. 2019).

Manual field mapping techniques allow sampling dedicated ecologically relevant variables in addition to vegetation cover, but are labor intensive, time consuming, and require expert knowledge in the field. Aerial and satellite remote-sensing approaches can reach centimeter spatial resolution, but such imagery is expensive and may not be available for a certain time period and region (e.g. due to cloud cover). Conducting UAV surveys in mountain terrain requires a trained and licensed pilot. UAV surveys may be limited in high mountain regions because of low air pressure, fast changing and extreme weather conditions, and the need for power supply in larger survey campaigns. In contrast, cameras for terrestrial photogrammetry are lightweight and can be used by trained nonprofessionals. Terrestrial photographs for photogrammetry can reach very high spatial resolution in the order of sub-centimeter and millimeters. The view angle can also be a lot shallower than from airborne products which view the surface predominantly from above. This makes terrestrial photogrammetry a promising approach for mapping vegetation cover and topography at plot

level in mountainous terrain (Eltner et al. 2016; Kaufmann 2012; Carrivick, Smith, and Quincey 2016).

The majority of studies mapping vegetation in remotely sensed imagery does not incorporate structural 3D information, which is originally available from the photogrammetric processing pipeline. Rugged terrain in particular, where much of the surface area is close to vertical or below overhangs, cannot be mapped using 2D raster approaches (Smith, Carrivick, and Quincey 2015). 3D-mapping approaches, such as laser scanning and photogrammetry, i.e. SfM-generated point clouds using vertical and oblique images, allow for detailed analyses that include mapping overhangs and 3D canopy structures (e.g. Rieke-Zapp, Rosenbauer, and Schlunegger 2009; Smith, Carrivick, and Quincey 2016). A comparison with terrestrial laser scanning (TLS)-mapped sites with dense vegetation cover demonstrates that SfM is able to represent the vegetation canopy in higher detail because the penetration of the laser beam into the canopy generates an underestimation of the height of the vegetation (Westoby et al. 2012). Vegetation extraction from topographic LiDAR point clouds is widely used and well established, although airborne LiDAR in a vegetation context is mainly concerned with forest cover and not mountain vegetation in particular (e.g. Kraus and Pfeifer 1998; Wehr and Lohr 1999; Luzum, Slatton, and Shrestha 2004; Silván-Cárdenas and Wang 2006). However, no color information is stored in the topographic LiDAR point attributes. Only recent technological advances merge imagery with point cloud data to produce colored point clouds (e.g. Lee, Lee, and Park 2017; Piewak et al. 2018). In contrast, photogrammetric point clouds come with built-in color information. Many workflows filter low vegetation out to improve terrain extraction (e.g. Wagner et al. 2004; Francesco Pirotti, Guarnieri, and Vettore 2013; Gruszczyński, Matwij, and Paweł 2017). Nevertheless, there are a few studies with an ecological focus that use 3D-mapping approaches such as SfM for characterizing micro-topography in detailed vegetation analysis (Lucieer et al. 2014; Niederheiser et al. 2018).

This study focuses (i) on vegetation detection in 3D photogrammetric point clouds, (ii) on the quantification of vegetation and non-vegetation cover, and (iii) on comparing three different methods of quantifying vegetated area in sample plots in alpine terrain. We

aim to evaluate how useful automatically derived topographic parameters from photogrammetric point clouds are for the assessment of vegetated areas and how they may support vegetation location interpretation by experts. We compared three different sampling methods and analyzed the derived vegetation cover in reference to local topographic parameters: automatically derived local green vegetation cover from photogrammetric point clouds, manually digitized vegetation cover based on orthoimages, and visual in-situ estimates.

2. Method and dataset

Based on photogrammetric point clouds attributed with RGB-color information and topographic parameters, we computed relative vegetation cover for each plot (in % of the total surface area including overhangs), where vegetation includes vascular plants, lichens and bryophytes. We describe the computation and attribution of the point clouds in sections 2.1 through 2.4 (cf. Niederheiser et al. 2018). From the attributed 3D point cloud, we extracted the vegetation points (Sect. 2.5). 3D vegetation surface area values were calculated after meshing. Digital surface meshing generates triangular faces based on the 3D points of the point cloud as vertices, where three neighboring vertices define one triangle of the mesh (Sect. 2.6). We compared those results derived from photogrammetry with *in-situ* estimates (according to Pauli et al. 2015) and manually digitized values from orthoimages (Sect. 2.7). Finally, we investigated the influence of

topographic parameters on vegetation cover with the help of linear mixed models (Sect. 2.8).

2.1. Study regions

Six study regions were selected, three in the temperate (European Alps) and three in the Mediterranean biome (Figure 1, Table 1). The study regions are part of the network of the Global Observation Research Initiative in Alpine Environments (GLORIA, www.gloria.ac.at), which has been monitoring vegetation changes on mountain summits since 2001 using a standardized method (Pauli et al. 2015). Each GLORIA study region consists of (usually) four summits across an elevation gradient from the tree line ecotone upwards. For this study, we surveyed the three highest summits and excluded the tree line ecotone because of abundant vegetation. The study sites selected in the two biomes and several elevations provides a diverse dataset with a large variety of location properties, including vegetation cover distributions (Supplementary Figure 3a, 4a, 5a, 6a for GLORIA reference data) and general topographies. On each summit, 16 clusters were installed in the four cardinal directions (North, East, South, and West) at 5 m, 25 m, 45 m, and 65 m below the highest summit point (HSP) (Supplementary Figure 1). Each 3×3 m cluster included nine 1 m² plots, with the four corner plots described and inventoried in detail. The vegetation cover in the clusters at 5 m below the HSP has been monitored every seven years since 2001, the other 12 clusters were newly installed for the current investigation.



Figure 1. Study regions in the temperate (Alps) and Mediterranean biome (Niederheiser et al. 2018, base map Bing Maps).

Table 1. Study regions, corresponding biome and elevations of the selected mountain peaks.

Region name	Code	Biome	Mountain peak elevations [m a.s.l.]
North-Eastern Alps/Hochschwab (Austria)	AT-HSW	Temperate (Alps)	2065, 2214, 2255
Western Alps/Valais (Switzerland)	CH-VAL	Temperate (Alps)	2550, 2989, 3212
Southern Alps/Dolomites (Italy)	IT-ADO	Temperate (Alps)	2463, 2757, 2893
Sierra Nevada (Spain)	ES-SNE	Mediterranean	2968, 3150, 3327
Crete/Lefka Ori (Greece)	GR-LEO	Mediterranean	1965, 2160, 2339
Central Apennines/Majella (Italy)	IT-CAM	Mediterranean	2511, 2635, 2737

2.2. Photogrammetric field setup and image acquisition

Photogrammetric acquisitions of the 249 clusters were set up in a standardized manner to facilitate comparable image acquisitions, automated processing, and repeatability (Supplementary Figure 2). Five Global Positioning System (GPS) loggers were placed in and around the clusters to generate GPS point clouds of which the median was used to derive an approximate absolute location of each cluster. A wooden target cube was placed at the center of each cluster for scaling and orientation of the photogrammetric point cloud. During the image acquisition, the camera was mounted on a 1.5 m long pole. For capturing nadir images, the camera was held approximately 2.5 m above the ground and moved across the plot in overlapping parallel strips, resulting in overlaps greater than 75%. Oblique images were captured by walking around the cluster and taking images from approximately 1.8 m and 2.4 m above the ground. The combinations of nadir and oblique images resulted in a dome-like structure of camera positions that minimized occlusions through overhangs and alongside-faces of rocks and boulders. Acquisition time per cluster including setup was less than one hour, even in rough terrain. Lens settings were fixed to the largest field of view (i.e. 18 mm to 24 mm) and autofocus as well as image stabilization was turned off to reduce the degrees of freedom during lens calibration. Further details on the acquisition process and hardware used can be found in Niederheiser et al. (2018).

2.3. Photogrammetric processing

Photogrammetric processing was done using the open-source software MicMac (IGN 2016) executed on the High-Performance Computing infrastructure (HPC) at the University of Innsbruck. The

photogrammetric processing chain resembled a standard photogrammetric workflow as can be found in the literature (e.g. Luhmann et al. 2013). First, all images of each location were screened to exclude blurred images and images that did not show enough of each plot's surface. Then, homologous tie-points were searched in each contrast-enhanced image, the tie-points were homogenized and image-matching between all images was performed by applying the Scale-Invariant Feature Transform algorithm (SIFT++) as implemented in the MicMac tool Tapioca (Pierrot-Deseilligny 2016). After the image matching, a self-calibration (MicMac tool Tapas) was conducted and a sparse point cloud reconstruction was performed. For the self-calibration we used a subset of acquired nadir images. Scaling and orientation were done manually, based on the wooden cube at the center of each cluster. The median GPS point of each location was used for absolute georeferencing of each plot. Dense-matching was performed last in the photogrammetric processing pipeline. Finally, the point clouds were manually cropped to the actual dimension of the cluster (3x3 m) using their corner points.

2.4. Topographic parameter derivation

All point cloud parameters were derived by automated processing. Topographic parameters were derived using SAGA GIS (System for Automated Geoscientific Analyses Geographic Information System, Conrad et al. 2015) and the proprietary LiS Toolbox (Laserdata GmbH 2015; Rieg et al. 2014). The final output of the photogrammetric workflow at sub-millimeter resolutions was downsampled to centimeter resolution to facilitate reasonable computation times for the database as a whole. Many plots included patches of higher growing vegetation (i.e. higher than a few decimeters), such as tall grasses, protruding flowers, and inflorescences. This presents

a special challenge as higher plant parts are prone to moving in the wind, which makes it difficult to reconstruct photogrammetrically with our setup. Instead of linear point cloud structures that would resemble blades of grass or stalks, disconnected artifacts of floating points were reconstructed. Some of these floating points actually produced quite large floating patches which we removed by a connected component analysis approach. In this approach we identified the largest connected components that we assumed resembled the ground segment. Smaller components that floated above the ground were discarded.

In line with the GLORIA field manual, the photogrammetric point clouds were also divided in nine 1×1 m plots. In GLORIA surveys these plots are sampled with an orthogonal view against the average terrain slope on the plots instead of a birds-eye view (Pauli et al. 2015). To achieve a corresponding segmentation, the point clouds were leveled horizontally, segmented by regularly dividing the outer edges, and finally reoriented into their original position.

We calculated per-point topographic indices, such as slope, aspect, roughness (SD_{RES} , SD_{Slope} , e_3), and topographic variability (omnivariance, λ_0) based on a spherical 0.05 m radius neighborhood, which we subsequently used for the vegetation segmentation. SD_{RES} is the standard deviation of the residual distance of 3D points to a fitted plane, SD_{Slope} is the standard deviation of the slope values of the included 3D points, and e_3 is the third eigenvector of a fitted plane in the neighborhood of a 3D point. In addition, single plane fittings for the complete 9 m² cluster areas and for the individual 1 m² plots were applied to classify the plots and corner areas to derive the same parameters as for the single points. We also computed the solar irradiation potential per point (for details, see Niederheiser et al. 2018).

2.5. Vegetation segmentation

The RGB color information of each 3D point was used to calculate three vegetation indices – Excess Green (ExG, Eq. (1)) (Woebbecke et al. 1995), Excess Green Minus Excess Red (ExGR, Eq. (2)) (Camargo Neto 2004), and Vegetation Index (VEG, Eq. (3)) (Hague, Tillett, and Wheeler 2006):

$$ExG = \frac{2G}{R + G + B} - \frac{R}{R + G + B} - \frac{B}{R + G + B} \quad (1)$$

$$ExGR = ExG - ExR = ExG - 1.4 * R - G \quad (2)$$

$$VEG = \frac{G}{R^a B^{1-a}} \text{ with } a = 2/3 \quad (3)$$

For the vegetation segmentation, a two-step supervised Random Forest (RF) classification was applied (Figure 2). Here we used the RF algorithm as implemented in the Python module Scikit-learn (Breiman 2001; Pedregosa et al. 2011).

RF has proved to be operationally applicable for remote-sensing classification tasks. RF provides information about the relevance of input features in the classification process (Breiman 2001), i.e., explaining which features are used and how much an input feature contributes to the derived model, while currently popular Deep Learning (DL) algorithms “offer little to no explanation/visibility into why specific features are selected over others” (Chakraborty et al. 2017) and are difficult for users to interpret. Chakraborty et al. (2017) have shown that the interpretability of a deep learning model is not a trivial task

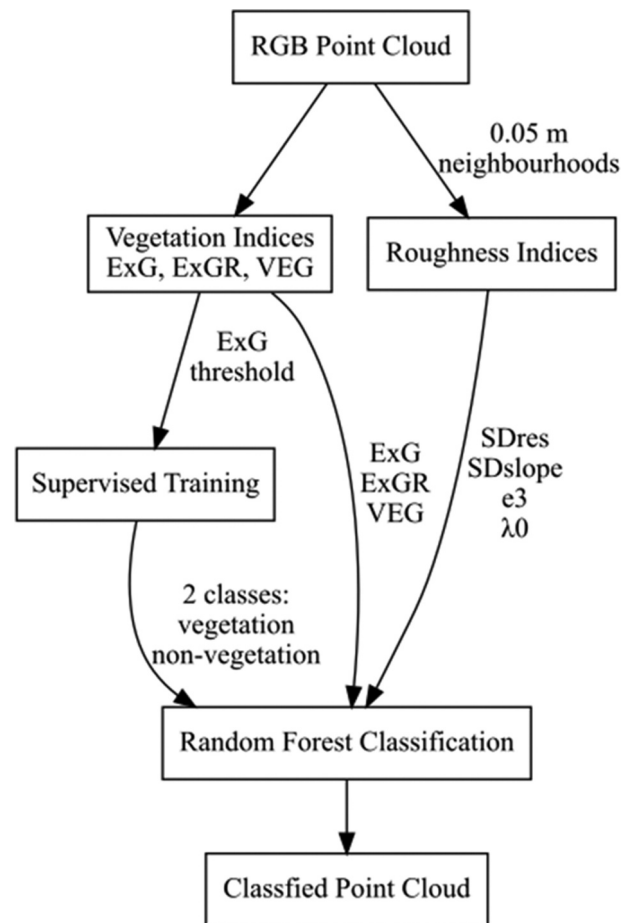


Figure 2. Random forest computation workflow.

and many different approaches exist. Recent publications also suggest that the quality of resulting DL classifications depends heavily on its parameterization. DL classifications outperform RF if large amounts of training data are available (Belgiu et al. 2016; Pirotti and Tonion 2019; Al-Najjar et al. 2019).

A conservative threshold of the ExG index was used in training to sample vegetation points based on empiric observations. Points with an ExG value >0.15 were classified as vegetation, points with an ExG value <0 as non-vegetation. These selected points were used to train a RF classifier (Breiman 2001). Included in the training were the three vegetation indices ExG, ExGR, and VEG, as well as the three roughness indicators SD_{RES} , SD_{Slope} , e_3 and the topographic variability parameter λ_0 .

We trained the RF classifier individually for each cluster. The combined relative number of points included in the training set of vegetation and non-vegetation ranged from just 15.35% to 86.04% by region (Figure 3). For each plot we grew 50 individual decision trees along the entropy criterion to minimize in-class uncertainties. We defined a maximum depth for each tree of five splits and set the maximum number of features considered for the best split at each node to the square root of the total number of features. Bootstrapping was used to build the decision trees. 37% of the data were left out during each bootstrap to be used for a generalized out-of-bag accuracy assessment (Breiman 1996). This accuracy assessment is a measure of how accurately the left-out data can be predicted based on each sub-sample

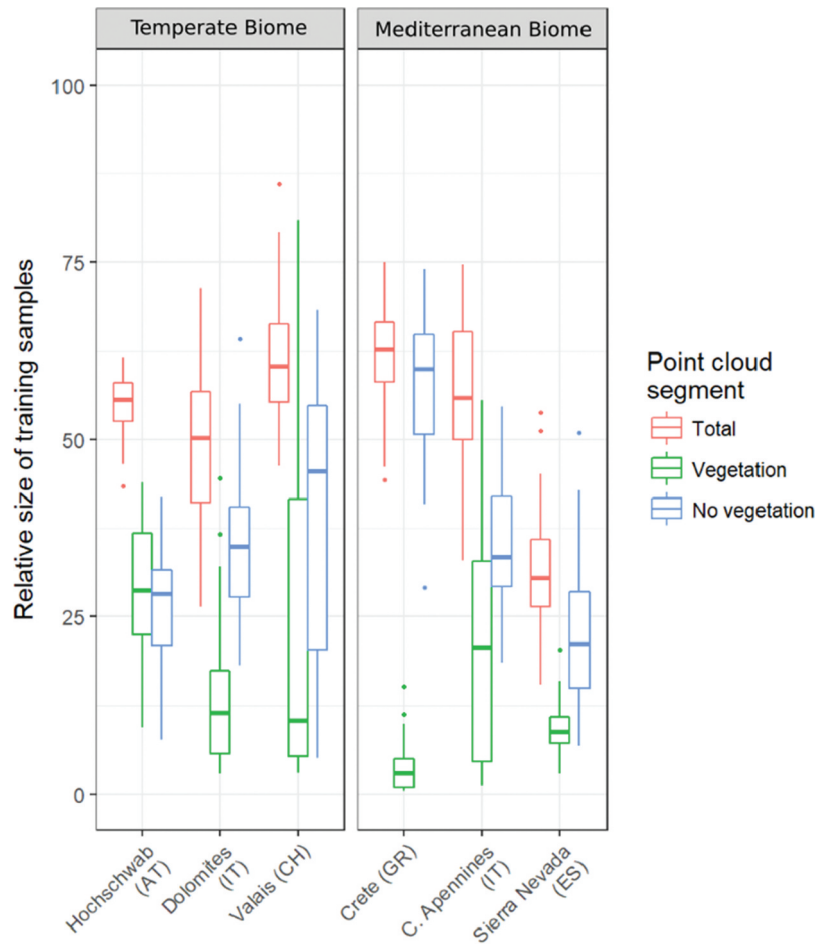


Figure 3. Relative sample sizes (i.e. number of points) per region and biome in [%] describing the proportion of points per plot included in the training sets (X% of 100%). Total (red) describes the whole training sample. Within the sample we distinguish vegetation points (green) and non-vegetation points (blue). Cumulative statistics per region (one value per plot) are shown. The thick lines are the median per region, the upper and lower box edges the 1st and 3rd quantile. The whiskers point to the minimum and maximum values, outliers are plotted as single points.

used for training. The points with an ExG value between 0 and 0.15 were classified using the individual RF classifiers.

2.6. 3D surface area of vegetation

In order to derive the 3D surface area of each cluster, we reconstructed the surfaces on the basis of the photogrammetric point clouds (Figure 4). Watertight mesh surfaces were reconstructed with the Screened Poisson Surface Reconstruction method, taking the points of the oriented point clouds as interpolation constraints (Kazhdan, Bolitho, and Hoppe 2006; Kazhdan and Hoppe 2013). This meant that the vertices of the reconstructed meshes were not the original points from the dense point cloud. Rather, the mesh reconstruction minimized the Root Mean

Square Error (RMSE) between the new surface and the original points. A density threshold trimmed the resulting surface meshes to the plot dimensions.

Then we assigned the vegetation classification of the point clouds to the mesh vertices by their nearest neighbors. If the majority of each triangle's vertices was classified as vegetation, then the triangular area was also defined as vegetated, otherwise it was defined as non-vegetated (Figure 5). Area values for each triangle of the mesh were calculated by simple trigonometry. They were in the order of mm² for each triangle.

2.7. Comparing photogrammetrically derived, manually digitized, and in-situ estimated vegetation cover

Using Linear Mixed-Effects Models (LMMs, "lmer" function of the R-Package 'lme4', Oberg and Mahoney 2007; Zuur et al. 2009), we compared the photogrammetrically derived 3D area estimates from the 3D meshes with *in-situ* vegetation cover estimates and with manually digitized estimates based on orthoimages. As the automated vegetation cover delineation relied strongly on the greenness of the single photogrammetric points, we compared it to aggregated covers of vascular plants, lichens, and bryophytes that are represented by green reflectance in the images. Comparisons were done for each biome separately and overall. Vegetation cover derived with one method was regressed against the cover as estimated by another method (fixed effect). We used plots nested in summits nested in regions as random intercept term (Oberg and Mahoney 2007; Zuur et al. 2009).

In-situ surface cover types (i.e. vascular plants, bryophytes, lichens, litter, scree, rock, open soil) were estimated visually in the four corner plots of each cluster, following Pauli et al. (2015). Surface cover types were manually digitized by drawing polygons on orthoimages of 207 3 × 3 m clusters using the GIS software ArcGIS 10.3 (ESRI 2015). These orthoimages were derived from the same input images used for the photogrammetric point clouds. After rectifying the orthoimages and fitting them to 3 × 3 m grids, the areas of the surface cover types in each 1 m² corner quadrat of each cluster were digitally polygonized in ArcMap (ESRI 2015, Figure 6). Areas smaller than 9 cm² were not delimited. For details, see Hofbauer (2018) and Klingraber (2018).

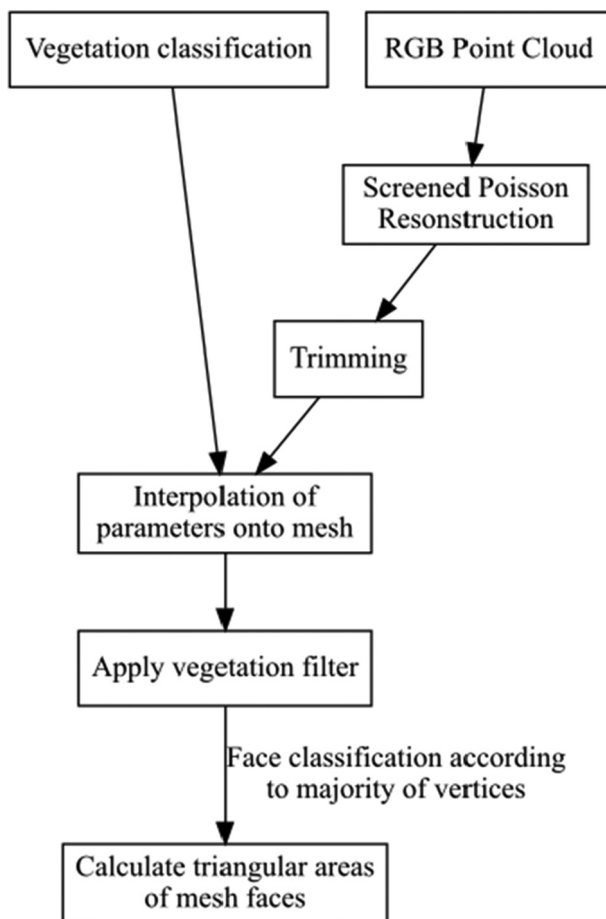


Figure 4. Workflow of surface area computation. RGB point clouds are meshed using Screened Poisson Reconstruction and the vegetation classes of the points are interpolated onto the mesh vertices using nearest neighbors. The faces of the meshes are classified by the majority of the classifications of the vertices.



Figure 5. Sample mesh with six vertices and four faces. Faces are classified according to the majority of their vertices, scale is in the order of mm².

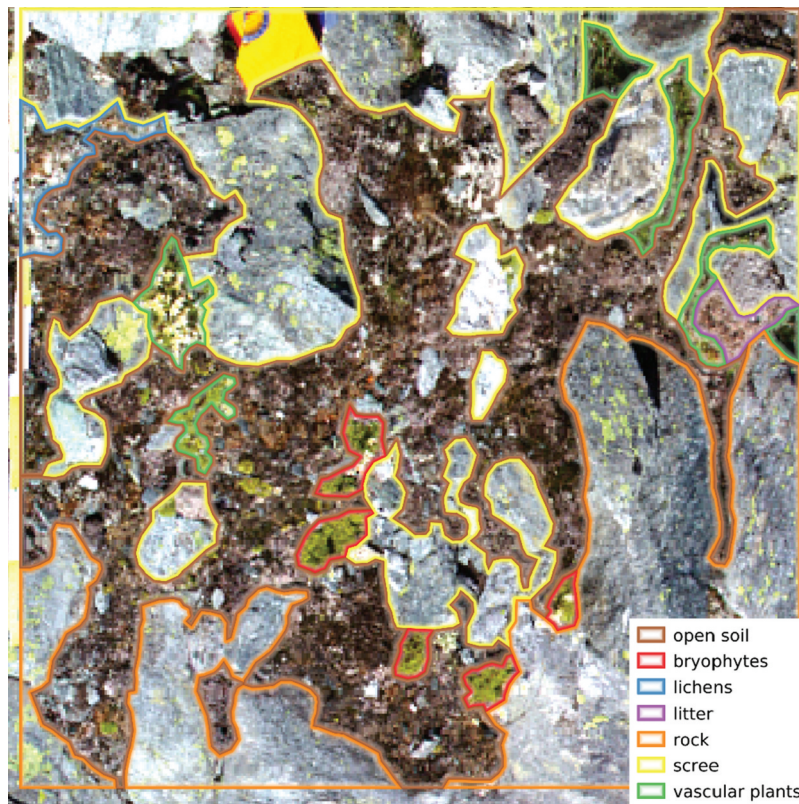


Figure 6. Orthoimage of a 1 × 1 m plot with surface types polygonized in the four corner plots (after Klinggraber 2018).

2.8. Assessing the effect of topographic parameters on vegetation cover

The effect of the topographic parameters of potential direct solar irradiation [kWh/m²], SD_{Slope} [°], λ_0 , aspect [°], slope [°], and elevation [m a.s.l.] on vegetation cover was assessed with regression models. The parameters were centered and scaled because of their very different original numeric scales. Centering is performed by subtracting the mean values of each parameter and scaling is done by dividing each

parameter by its standard deviation. Collinearity of parameters was tested with the corvif function (R Core Team 2018; Zuur et al. 2009). The parameters of potential diffuse solar irradiation, e_3 , and SD_{RES} , which returned collinearity values >2, were removed from the model (Zuur et al. 2009). Owing to the spatial structure of the dataset, we used LMMs with the topographic parameters as fixed effects and clusters nested in summits nested in regions nested in biomes as random intercept term.

To assess the impact of the individual features used in the LMMs, we applied a stepwise exclusion of single factors and compared the Akaike Information Criteria (AIC) of the reduced models to the AIC of the full model (AIC difference, Zuur et al. 2009). The AIC measures fit and complexity of a model. A lower AIC indicates a better fit of the model. The larger the difference between the AICs of two models, the greater the impact of a missing factor in the reduced model. Here the AIC difference (AIC diff.) is the AIC of the full model, subtracted from the AIC of a reduced model. A positive value indicates a worse fit of the reduced model than the full model if the respective factor was removed. For this comparison, the models were fitted by maximum likelihood estimation. In addition, we compared the relative likelihoods (Rel. likelihood) of the reduced models in relation to the full model ((4), Burnham, Anderson, and Huyvaert 2011). A low relative likelihood indicates a poorer fit of the reduced model than the full model.

$$e^{-\frac{1}{2} \times (AIC_{\text{of reduced model}} - AIC_{\text{of full model}})} \quad (4)$$

Marginal and conditional R^2 for LMMs were calculated following Nakagawa and Schielzeth (2013). The marginal R^2 describes how well the model fits the data based on the association with the fixed effects – it describes the proportion of variance explained by the fixed effects. The conditional R^2 describes how well the model fits the data based on the association with the fixed effects plus the random effects. The difference between marginal and conditional R^2 reflects the variability in the random effects (Nakagawa and Schielzeth 2013).

3. Results

First, we describe the results of the RF classification (Sect. 3.1). Second, we present a summary of the topographic dependencies of the vegetation cover modeled by LMMs (Sect. 3.2). Third, we compare the vegetation cover values based on the photogrammetric models with *in-situ* estimates and manually digitized results (Sect. 3.3).

3.1. Random forest vegetation classification results

Feature importance for all included features in the RF classification is directly included in the results of the RF algorithm. The most important features for the

vegetation cover classification were the RGB-based indices ExG, VEG, and ExGR (Figure 7(a)). This was true for both biomes. The roughness features were less important. The topographic parameters did not characterize vegetation points very well and thus did not seem to have a strong effect on the vegetation cover delineation (Figure 7(a, b)). This conclusion is supported by the fact that a RF classification based on roughness values alone did not yield satisfactory results. Using all mentioned indices in conjunction (ExG, VEG, ExGR, SD_{RES} , SD_{Slope} , e_3 , λ_0), the global mean out-of-bag error and the mean out-of-bag error for the temperate and the Mediterranean biome were around zero. Because RFs do not overfit (Breiman 2001; Belgiu and Drăguț 2016), the low out-of-bag errors suggest very good fits of the models. However, the errors do not allow for differentiating performance between the temperate and the Mediterranean biome.

3.2. Topographic factors associated with vegetation cover

Overall, the most important topographic factors, based on LMMs, for modeling plot-wise vegetation cover were SD_{Slope} , elevation, aspect, and mean potential direct solar irradiation (see Table 2). In the temperate biome (Alps), the most important factors were elevation, mean potential direct solar irradiation, λ_0 , and aspect. In the Mediterranean biome, the most important factors were SD_{Slope} , aspect and mean potential direct solar irradiation. The fixed effects explained between 19.6% and 37.3% of the total variance of the models (marginal R^2 , Table 2). Between 87% and 92.5% of the variance of the models can be explained by the combined fixed and random factors (conditional R^2 , Table 2).

3.3. Comparison between *in-situ* estimates, manually digitized, and photogrammetrically derived values of vegetation cover

We used mixed-effect models to determine how well the vegetation cover estimates of the different methods match. The vegetation cover values estimated with the different methods were significantly positively correlated (LMMs, Figure 8, Table 3). Marginal R^2 ranged between 60.5% and 88.5% and conditional R^2 between

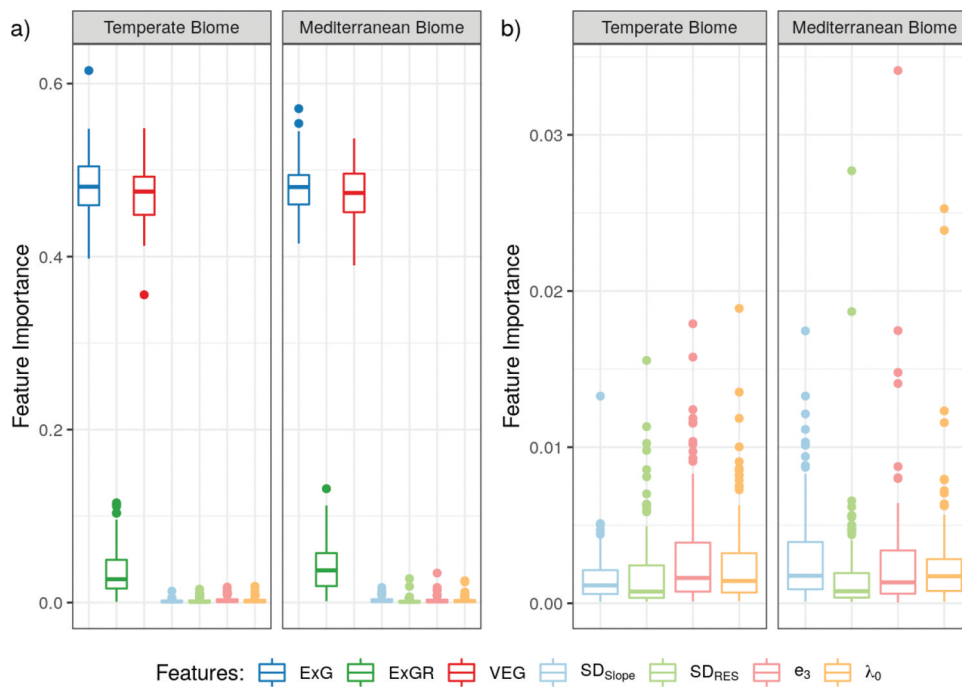


Figure 7. (a) Feature importance, (b) Feature importance of topographic indices only. ExG = Excess Green, ExGR = Excess Green Minus Excess Red, VEG = Vegetation Index, SD_{Slope} = Standard deviation of slope, SD_{RES} = Standard deviation of the residual distance of 3D points to a fitted plane, e_3 = 3rd eigenvector, λ_0 = Omnivariance. Cumulative statistics per biome (one value per plot) are shown. The thick lines are the median per feature, the upper and lower box edges the 1st and 3rd quartile. The whiskers point to the minimum and maximum values, outliers are plotted as single points.

87.2 and 93.5%. The strongest correlation was found between *in-situ* estimates and manually digitized GIS results when considering fixed effects only (marginal $R^2 > 0.86$), and was highest between manually digitized GIS results and photogrammetrically derived vegetation cover when considering fixed and random effects together (conditional $R^2 > 0.91$). Correlation between manually digitized results and photogrammetrically derived vegetation cover ranked second (marginal $R^2 < 0.77$) and correlation between *in-situ* estimates and photogrammetrically derived vegetation cover ranked third (marginal $R^2 < 0.67$). Correlations with photogrammetrically derived vegetation cover values in the Mediterranean biome were generally stronger than in the temperate biome (conditional $R^2 > 0.89$). Correlations between *in-situ* estimates and manually GIS digitized values were stronger in the temperate biome than in the Mediterranean biome (conditional $R^2 = 0.91$). On average, photogrammetrically derived cover values were lower than both *in-situ* estimates (Figure 8(a)) and values derived

from manual digitizing (Figure 8(c)), except in cases of very low vegetation cover, where the photogrammetrically derived values overestimate vegetation cover, especially in the Mediterranean biome. *In-situ* cover estimates were higher than cover values derived from manual digitizing with vegetation cover $< 30\%$, and lower at higher vegetation covers (Figure 8(b)).

4. Discussion

4.1. Random forest classification

RF classification was applied for the classification of vegetation points. The low feature importance values of the topographic features suggest that they do not add relevant additional information for vegetation cover description by the classifier. Rather, the performance of the classifiers relied predominantly on the green color of vegetation, which was largely influenced by the time of year (i.e. the vegetation period) and shadowing effects. If vegetation was not green, it was not recognized in the training stage, which

Table 2. Results of the AIC comparison of the full model to reduced models. AIC diff. is the AIC of the reduced model minus the AIC of the full model. Rel. likelihood was calculated as $e^{-\frac{1}{2} * (AIC_{reducedmodel} - AIC_{fullmodel})}$. Models where the full model is better than the reduced model, i.e. the omitted factor has a significant impact, have positive AIC diff. values and are printed in bold. SD_{Slope} = Standard deviation of slope; λ_0 = Omnivariance.

Model	Overall			Temperate Biome		Mediterranean Biome	
	AIC	AIC diff.	Rel. likelihood	AIC	AIC diff.	AIC	AIC diff.
Full Model	1,837	-	0.000	890	-	842	-
Mean potential direct solar irradiation during vegetation period	1,839	2.07	0.355	895	4.63	843	0.60
SD_{Slope}	1,850	13.11	0.001	890	-0.80	858	15.69
λ_0	1,836	-0.97	1.625	893	2.86	842	-0.74
Aspect	1,847	9.86	0.007	892	1.87	845	2.43
Slope	1,835	-2.00	2.718	889	-1.65	842	-0.68
Elevation	1,844	10.10	0.006	902	11.12	840	-1.82
Observations		959			395		564
Marginal R ²		0.312			0.373		0.196
Conditional R ²		0.912			0.870		0.925

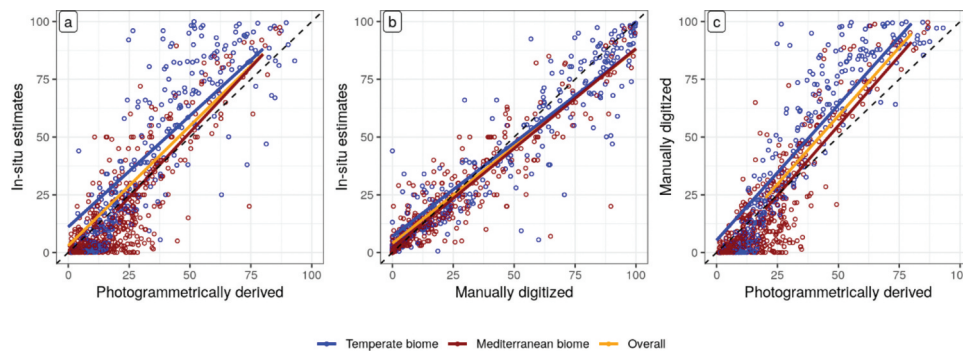


Figure 8. Correlations between the different vegetation cover estimation methods: (a) *in-situ* estimates vs photogrammetrically derived; (b) *in-situ* estimates vs manually digitized; (c) manually digitized vs photogrammetrically derived. The 1:1 line is shown in black dashes.

Table 3. Correlations of photogrammetrically derived *in-situ* estimates, and manually digitized vegetation cover values for the temperate and Mediterranean biomes separately, as well as overall. Shown are the fixed effects (marginal R^2) and combined fixed and random effects (conditional R^2) of linear mixed-effect models (LMMs), computed using the function “lmer” in the R-package “lme4” (Bates et al. 2015). P-values were computed via Wald-statistics approximation (Lüdtke 2018); CI = confidence interval.

Biome	Comparison	Coefficient	CI	p-Value	N	Marginal R^2	Conditional R^2
Overall	3D photogrammetric – manually digitized	1.19	1.14–1.23	<0.001	779	0.756	0.929
	3D photogrammetric – <i>in situ</i> estimated	1.04	0.99–1.09	<0.001	779	0.661	0.882
	manually digitized – <i>in situ</i> estimated	0.84	0.81–0.87	<0.001	779	0.885	0.914
Temperate	3D photogrammetric – manually digitized	1.17	1.10–1.24	<0.001	320	0.763	0.919
	3D photogrammetric – <i>in situ</i> estimated	0.96	0.88–1.05	<0.001	320	0.605	0.872
	manually digitized – <i>in situ</i> estimated	0.81	0.77–0.86	<0.001	320	0.866	0.913
Mediterranean	3D photogrammetric – manually digitized	1.21	1.15–1.26	<0.001	459	0.723	0.935
	3D photogrammetric – <i>in situ</i> estimated	1.13	1.06–1.20	<0.001	459	0.669	0.891
	manually digitized – <i>in situ</i> estimated	0.87	0.82–0.91	<0.001	459	0.868	0.894

applied a threshold of the ExG index above which points very likely belonged to vegetation. This was especially important for the arid Mediterranean regions and could be mitigated by manually classifying a number of vegetated areas in a subset of plots. However, this would have counteracted the benefits of the automated approach, which was to minimize subjective user input and to speed up the training process. The feature importance of the vegetation indices used for the RF classification varied depending on the type of green vegetation (i.e. onsite visits revealed that patches of grass or moss have a different texture and topographic micro-scale variance than, for example, lichens on rocks). Lichens on rocks and rock surfaces basically have the same topographic properties. Thus, the color-based vegetation indices could have had a significant feature importance (Figure 7(a, b)). In general, the RF classification results revealed very low out-of-bag error. Overfitting could be ruled out because of the large number of random iterations and because RFs always converge (Breiman 2001; Belgiu and Lucian 2016). The low errors confirm RF as very suitable for vegetation classification, which is in line with numerous studies in

which RFs outperform other classifiers for this task (e.g. Feng, Liu, and Gong 2015; Pádua et al. 2019).

4.2. Photogrammetrically derived vegetation cover and topographic dependency in biomes by linear mixed model analysis

Topographic parameters were an asset when it came to explaining the distinct variation in vegetation cover found between biomes, regions, summits, elevation, and aspects (see Supplementary Figure 3b, 4b, 5b, 6b). Confirming Winkler et al. (2016), relative vegetation cover was less in the Mediterranean biome than in the temperate biome (Alps). In addition, relative vegetation cover decreased with increasing elevation and was higher on eastern and southern aspects than on northern and western ones. However, general statements should be made with caution as the effects varied between the biomes and regions.

Vegetation cover in the Mediterranean mountains was independent of elevation (LMMs, Table 2) for several reasons: First, vegetation cover in our clusters is generally low in the Mediterranean biome because of limited availability of water. Second, roughness

seemed to be important for vegetation cover classification (SD_{Slope} , Table 2). This contrasts with the temperate biome, where elevation dominated over roughness (λ_0 , Table 2). The temperate biome, especially, included summits of great variety, from very green and grassy to bare, rough, and blocky, which largely follows the elevation gradient from the lower alpine upwards.

About a third of the variation in vegetation cover could be explained by the topographic parameters (Table 2). This suggests that there might be additional auxiliary variables (e.g. from climate data, such as temperature or precipitation), which could help to further differentiate location properties of different biomes. Especially the arid regions in the Sierra Nevada and on Crete are influenced by a dry summer season, whereas in the Alps the precipitation maximum occurs in summer (Peel, Finlayson, and McMahon 2007). Precipitation data should be included in future research, although reliable data from high elevations are scarce and are difficult to measure reliably in mountain areas (Félix and Konzelmann 2016). Also, the effect of snow cover duration plays an important role for alpine vegetation and is bound to change in a warming climate (Liberati et al. 2019). Here we only used the potential solar irradiation for a vegetation period from June to September as an approximation for all regions. A more region-specific irradiation model could improve the explained variation in our model. The large proportion of explained variation by the random effects supports the argument that overlying regional patterns greatly influence the observed vegetation cover.

4.3. Comparison of the results between the different sampling methods for vegetation cover

The photogrammetrically derived vegetation cover values tended to underestimate cover with abundant vegetation and to overestimate sparse vegetation cover when compared to the *in-situ* estimates and manually digitized values (Figure 8). Differences of 25% and greater were observed in 9.6% of the cases for the photogrammetric vs. *in-situ* comparison, in 11.1% of the cases for the manually digitized vs. automated photogrammetric 3D point cloud approach, and in 2.9% for the *in-situ* vs. manually digitized

approach. Most of these outliers were encountered for the Swiss and Austrian regions (CH-VAL and AT-HSW), with over half of the cases found in these regions. These were also the two generally greenest regions, with the most abundant vegetation in the form of grasses, sedges, and dwarf shrubs, which made the photogrammetric reconstruction difficult. The difference between marginal and conditional R^2 was greatest for the photogrammetric dataset vs. *in-situ* estimates, second for the manual GIS digitization vs. the automated photogrammetric approach, and least for the *in-situ* estimates vs. the manual digitization. Nevertheless, the high correlations (p-values < 0.001) between the photogrammetric and the other two datasets, the *in-situ* estimates and the manually digitized values, confirm that the photogrammetric method is an independent alternative and a repeatable tool for estimating vegetation cover based on photographs (Table 3).

The *in-situ* estimates and the manually digitized results largely depend on the manual operator, even though the standardized GLORIA Field Manual (Pauli et al. 2015) seeks to minimize these effects by multiple surveys of the same plot by different researchers at the same time. An observer error study quantified differences in *in-situ* plant species cover estimates between observers in three regions in the Alps and Carpathians (including one of our study regions, AT-HSW; Futschik et al. 2020). However, that study investigated disagreement in cover estimates of each plant species, while we took all vascular plants together here. Even so, we suppose that their results can be transferred to our study. Mean percentage difference of plant species cover estimates from the consensus estimate (*i.e.*, the mean across all observers) of 28 observers ranged from ca. 9–18% and was significantly and consistently far smaller than changes in cover over time. The greatest source of disagreement by far among observers was the amount of cover of a given species with the percentage error decreasing with increasing species cover, followed by observer identity (Futschik et al. 2020). In contrast, for manual digitizing, the resolution and quality of the orthophotos may be more important than either cover or researcher, because these features are essential to reliably distinguishing vascular plants from lichens or bryophytes.

5. Conclusion

The results of the RF classification confirm RFs as a suitable tool for vegetation classification. The technique worked for our application and the low out-of-bag errors suggest very good results. However, the heavy dependency on the greenness of vegetation turned out to be problematic in the arid climate in some of our research areas where vegetation was often already dry. The applied training approach of using an ExG threshold focused on the greenness, but the idea was to include the underlying topography in the RF classifier to catch non-green vegetation in a second step. The relative values of feature importance indicate that the potential of the inclusion of topographic parameters was not utilized by the classifier. Further research needs to be done on the micro-topographic effects included in the RF vegetation segmentation. The different micro-topographies, i.e. surface and canopy structure of grass, forb, dwarf shrub, moss, and lichens, would be useful to distinguish between the vegetation types in the point cloud for botanical and ecological interpretation. Moreover, RGB information has its own limitations as it is sensible to variations in lighting conditions and shadows, which play an important role for the interpretation and derivations of vegetation indices. A change of the color space from RGB to HSI (Hue Saturation Intensity) for shadow segmentation could help to mitigate such effects and facilitate shadow segmentation (e.g. Laliberte, Rango, and Fredrickson 2006; Tsai 2006). It may also be favorable to capture the images under diffuse lighting conditions to mitigate saturation effects on light surfaces caused by strong direct solar irradiation. However, this is not feasible in large acquisition campaigns as conducted in this project (Niederheiser et al. 2018). A near-infrared channel for vegetation discovery in images or even hyperspectral imaging techniques could improve detection results and be incorporated into the photogrammetric workflow. Specialized cameras using CIR (Color Infrared) or V/NIR (Visible/Near Infrared) to provide spectral information with greater discriminatory power for vegetation are becoming readily available and affordable.

Our application of LMMs utilized the topographic parameters and was able to reveal dependencies in the two biomes, such as elevation and aspects. The LMMs were able to explain between 87% and 92.5%

of variance. However, the large difference between marginal R^2 and conditional R^2 suggests that further parameters might exist that could aid the characterization of both biomes.

The comparison of all three surveying methods showed that the *in-situ* approach requires the most botanical knowledge and thus needs to be done by botany experts. It represents the most detailed reference for botanical and ecological analysis and fully relies on the expert's knowledge in the field yielding the most detailed botanical insight. But *in-situ* estimates are only taken once and cannot be repeated at a later time under the exact same circumstances (e.g. weather, method, trampling, etc.). In contrast, the image acquisition for photogrammetry and orthoimages can be done by trained non-experts who are handy with camera equipment and photogrammetric software. Images captured for the photogrammetric method and manual digitization can be analyzed multiple times with different approaches, taking advantage of improved and updated algorithms. Automation makes data processing and classification repeatable. Combining new and historic images can result in time-series analysis, i.e. change detection. For upscaling, more sophisticated knowledge about workflow automation is needed. The same is true for orthoimage generation. The vegetation classification and cover derivation are purely a computer vision problem.

Currently the presented automated workflow can reliably distinguish between vegetation and non-vegetation by relying on greenness. The differentiation of plant species requires deeper interpretation, as is possible by *in-situ* estimates and by manual digitization for easily distinguishable species and with sufficient image resolution. The main advantage of the photogrammetric method is the direct spatial link to topographic parameters, which also provide a general picture of vegetation cover. It can be applied on multiple plots or area-wide and is transferable to other locations. The orthoimages are also a result of the photogrammetric workflow, which can be used for visual image interpretation and detailed plant species definition.

From a technical, i.e. mapping method, perspective, it would be interesting to see how well hand-held topographic LiDAR devices perform for micro-topography mapping purposes (Kersten, Lindstaedt, and Starosta 2018). Hand-held devices are usually

lightweight enough to carry to mountain summits. Future work should focus on upscaling the approach for mapping whole summits, e.g. using Unmanned Aerial Vehicles (UAV). If wind conditions allow UAV flights, this would also be an alternative survey concept since they cost less than a professional DSLR (Digital Single-Lens Reflex) camera. However, you cannot control the UVA camera's lens parameters, as the camera typically is fully automatic, but camera resolutions are very high (4 K), and photogrammetric software has become very easy to use and can handle distortions much better (e.g. O'Connor, Smith, and James 2017).

Acknowledgements

This work has been conducted within the project MEDIALPS (Disentangling anthropogenic drivers of climate change impacts on alpine plant species), which was funded by the Earth System Sciences Program of the Austrian Academy of Sciences. We thank all field workers who helped gather *in-situ* vegetation data and photogrammetric data.


Part of the computational results presented here were achieved using the HPC infrastructure LEO of the University of Innsbruck. The LIS Toolbox was kindly provided by Laserdata GmbH, Innsbruck.

English editing was done by Brigitte Scott.

Disclosure statement

No potential conflict of interest was reported by the authors.

ORCID

R. Niederheiser  <http://orcid.org/0000-0002-9767-1307>
 M. Winkler  <http://orcid.org/0000-0002-8655-9555>
 A. Lamprecht  <http://orcid.org/0000-0002-8719-026X>
 L. Nicklas  <http://orcid.org/0000-0002-9337-4153>
 P. Nyktas  <http://orcid.org/0000-0002-9571-1440>
 H. Pauli  <http://orcid.org/0000-0002-9842-9934>
 A. Stanisci  <http://orcid.org/0000-0002-5302-0932>
 K. Steinbauer  <http://orcid.org/0000-0002-3730-9920>
 J.-P. Theurillat  <http://orcid.org/0000-0002-1843-5809>
 P. Vittoz  <http://orcid.org/0000-0003-4218-4517>
 M. Rutzinger  <http://orcid.org/0000-0001-6628-4681>

References

Al-Najjar, H. A. H., B. Kalantar, B. Pradhan, V. Saeidi, A. A. Halin, N. Ueda, and S. Mansor. 2019. "Land Cover Classification from Fused DSM and UAV Images Using Convolutional

- Neural Networks." *Remote Sensing* 11 (12): 1–18. doi:10.3390/rs11121461.
- Bates, D., M. Mächler, B. Bolker, and S. Walker. 2015. "Fitting Linear Mixed-Effects Models Using Lme4." *Journal of Statistical Software* 67 (1): 1–48. doi:10.18637/jss.v067.i01.
- Belgiu, M., and D. Lucian. 2016. "Random Forest in Remote Sensing: A Review of Applications and Future Directions." *ISPRS Journal of Photogrammetry and Remote Sensing* 114: 24–31. doi:10.1016/j.isprsjprs.2016.01.011.
- Breiman, L. 1996. *OUT-OF-BAG ESTIMATION*. Berkeley, CA, USA. <http://www.stat.berkeley.edu/~breiman/OOBestimation.pdf>.
- Breiman, L. 2001. "Random Forests." *Machine Learning* 45 (1): 5–32. doi:10.1023/A:1010933404324.
- Burnham, K. P., D. R. Anderson, and K. P. Huyvaert. 2011. "AIC Model Selection and Multimodel Inference in Behavioral Ecology: Some Background, Observations, and Comparisons." *Behavioral Ecology and Sociobiology* 65: 23–35. doi:10.1007/s00265-010-1029-6.
- Camargo Neto, J. 2004. *A Combined Statistical-Soft Computing Approach for Classification and Mapping Weed Species in Minimum-Tillage Systems*. USA: University of Nebraska. doi:10.1016/B978-012397720-5.50034-7.
- Carrivick, J. L., M. W. Smith, and D. J. Quincey. 2016. *Structure from Motion in the Geosciences*. Oxford, UK: John Wiley & Sons.
- Chakraborty, S., R. Tomsett, R. Raghavendra, D. Harborne, M. Alzantot, F. Cerutti, M. Srivastava, et al. 2017. "Interpretability of Deep Learning Models: A Survey of Results." In *2017 IEEE SmartWorld, Ubiquitous Intelligence & Computing, Advanced & Trusted Computed, Scalable Computing & Communications, Cloud & Big Data Computing, Internet of People and Smart City Innovation (SmartWorld/SCALCOM/UIC/ATC/CBDCOM/IOP/SCI)*, 1–6. IEEE, San Francisco, CA. doi:10.1109/UIC-ATC.2017.8397411.
- Conrad, O., B. Bechtel, M. Bock, H. Dietrich, E. Fischer, L. Gerlitz, J. Wehberg, V. Wichmann, and J. Böchner. 2015. "System for Automated Geoscientific Analyses (SAGA)." doi:10.5194/gmd-8-1991-2015.
- Eltner, A., A. Kaiser, C. Castillo, G. Rock, F. Neugirg, and A. Antonio. 2016. "Image-Based Surface Reconstruction in Geomorphometry-Merits, Limits and Developments." *Earth Surface Dynamics* 4 (2): 359–389. doi:10.5194/esurf-4-359-2016.
- ESRI. 2015. "ArcGIS 10.3." <https://desktop.arcgis.com/en/arcmap/10.3/main/get-started/whats-new-in-arcgis.htm>.
- Félix, C., and T. Konzelmann. 2016. "Surface Precipitation Measurements." In *From Weather Observations to Atmospheric and Climate Sciences in Switzerland*, edited by S. Willemse and M. Furger. Zurich: vdf Hochschulverlag AG an der ETH Zürich (pp. 125–140).
- Feng, Q., J. Liu, and J. Gong. 2015. "UAV Remote Sensing for Urban Vegetation Mapping Using Random Forest and Texture Analysis." *Remote Sensing* 7 (1): 1074–1094. doi:10.3390/rs70101074.
- Friedmann, B., H. Pauli, M. Gottfried, and G. Grabherr. 2011. "Suitability of Methods for Recording Species Numbers and

- Cover in Alpine Long-Term Vegetation Monitoring." *Phytocoenologia* 41 (2): 143–149. doi:10.1127/0340-269X/2011/0041-0480.
- Futschik, A., M. Winkler, K. Steinbauer, A. Lamprecht, S. B. Rumpf, P. Barančok, A. Palaj, M. Gottfried, and H. Pauli. 2020. Disentangling Observer Error and Climate Change Effects in Long-term Monitoring of Alpine Plant Species Composition and Cover. *Journal of Vegetation Science* November Edited by Sándor Bartha. doi:10.1111/jvs.12822.
- Gruszczyński, W., W. Matwij, and Ć. Paweł. 2017. "Comparison of Low-Altitude UAV Photogrammetry with Terrestrial Laser Scanning as Data-Source Methods for Terrain Covered in Low Vegetation." *ISPRS Journal of Photogrammetry and Remote Sensing* 126: 168–179. doi:10.1016/j.isprsjprs.2017.02.015.
- Hague, T., N. D. Tillett, and H. Wheeler. 2006. "Automated Crop and Weed Monitoring in Widely Spaced Cereals." *Precision Agriculture* 7 (1): 21–32. doi:10.1007/s11119-005-6787-1.
- Hofbauer, H. 2018. *Mapping Surface Types in High Mountain Environments of the Alps*. Vienna, Austria: University of Natural Resources and Life Sciences Vienna (BOKU), Bachelor Thesis
- IGN, Institut national de l'information géographique et forestière. 2016. "Micmac." <https://culture3d:culture3d@geoportail.forge.ign.fr/hg/culture3d>.
- Kaufmann, V. 2012. "The Evolution of Rock Glacier Monitoring Using Terrestrial Photogrammetry: The Example of Äusseres Hochebenkar Rock Glacier (Austria)." *Austrian Journal of Earth Sciences* 105 (2): 63–77.
- Kazhdan, M., and H. Hoppe. 2013. "Screened Poisson Surface Reconstruction." *ACM Transactions on Graphics* 32 (3): 1–13. doi:10.1145/2487228.2487237.
- Kazhdan, M., M. Bolitho, and H. Hoppe. 2006. "Poisson Surface Reconstruction." *Eurographics Symposium on Geometry Processing*. Cagliari, Sardinia. <http://www.cs.jhu.edu/~misha/MyPapers/SGP06.pdf>.
- Kersten, T. P., M. Lindstaedt, and D. Starosta. 2018. "Comparative Geometrical Accuracy Investigations of Hand-held 3D Scanning Systems - an Update." *ISPRS - International Archives of the Photogrammetry, Remote Sensing and Spatial Information Sciences XLII-2* (2): 487–494. doi:10.5194/isprs-archives-XLII-2-487-2018.
- Klingraber, B. 2018. *Comparing Two Methods of Recording the Top Cover of Surface Types in Permanent Plots on GLORIA Summits in Mediterranean Regions*. Vienna, Austria: University of Natural Resources and Life Sciences Vienna (BOKU), Bachelor Thesis.
- Körner, C., ed. 2003. *Alpine Plant Life*. 2nd ed. Heidelberg: Springer.
- Kraus, K., and N. Pfeifer. 1998. "Determination of Terrain Models in Wooded Areas with Airborne Laser Scanner Data." *ISPRS Journal of Photogrammetry and Remote Sensing* 53 (4): 193–203. doi:10.1016/S0924-2716(98)00009-4.
- Laliberte, A. S., A. Rango, and L. Fredrickson. 2006. "Separating Green and Senescent Vegetation in Very High Resolution Photography Using an Intensity-Hue-Saturation Transformation and Object Based Classification." *Proceedings of ASPRS 2006 Annual Conference Reno, Nevada*.
- Laserdata, G. 2015. "LIS." *Official Website*. <http://www.laserdata.at/>.
- Lee, G.-M., J.-H. Lee, and S.-Y. Park. 2017. "Calibration of VLP-16 Lidar and Multi-View Cameras Using a Ball for 360 Degree 3D Color Map Acquisition." In *2017 IEEE International Conference on Multisensor Fusion and Integration for Intelligent Systems (MFI)*, 64–69. IEEE, Daegu, South Korea. doi:10.1109/MFI.2017.8170408.
- Liberati, L., S. Messerli, M. Matteodo, and P. Vittoz. 2019. "Contrasting Impacts of Climate Change on the Vegetation of Windy Ridges and Snowbeds in the Swiss Alps." *Alpine Botany*, September, 1–11. doi:10.1007/s00035-019-00223-5.
- Lucieer, A., D. Turner, D. H. King, and S. A. Robinson. 2014. "Using an Unmanned Aerial Vehicle (UAV) to Capture Micro-Topography of Antarctic Moss Beds." *International Journal of Applied Earth Observation and Geoinformation* 27 (PARTA): 53–62. Elsevier B.V. doi:10.1016/j.jag.2013.05.011.
- Lüdecke, D. 2018. "SjPlot: Data Visualization for Statistics in Social Science." doi:10.5281/zenodo.1308157.
- Luhmann, T., S. Robson, S. Kyle, and J. Boehm. 2013. *Close-Range Photogrammetry and 3D Imaging*. Berlin, Boston: DE GRUYTER. doi:10.1515/9783110302783.
- Luzum, B. J., K. C. Slatton, and R. L. Shrestha. 2004. "Identification and Analysis of Airborne Laser Swath Mapping Data in a Novel Feature Space." *IEEE Geoscience and Remote Sensing Letters* 1 (4): 268–271. doi:10.1109/LGRS.2004.832229.
- Mohapatra, J., C. P. Singh, M. Hamid, A. A. Khuroo, A. H. Malik, and H. A. Pandya. 2019. "Assessment of the Alpine Plant Species Biodiversity in the Western Himalaya Using Resourcesat-2 Imagery and Field Survey." *Journal of Earth System Science* 128 (7): 189. doi:10.1007/s12040-019-1219-1.
- Nakagawa, S., and H. Schielzeth. 2013. "A General and Simple Method for Obtaining R² from Generalized Linear Mixed-Effects Models." *Methods in Ecology and Evolution* 4 (2): 133–142. doi:10.1111/j.2041-210x.2012.00261.x.
- Niederheiser, R., M. Rutzinger, M. Bremer, and V. Wichmann. 2018. "Dense Image Matching of Terrestrial Imagery for Deriving High-Resolution Topographic Properties of Vegetation Locations in Alpine Terrain." *International Journal of Applied Earth Observation and Geoinformation* 66 (April): 146–158. Elsevier. doi:10.1016/j.jag.2017.11.011.
- O'Connor, J., M. J. Smith, and M. R. James. 2017. "Cameras and Settings for Aerial Surveys in the Geosciences: Optimising Image Data." *Progress in Physical Geography* 41 (3): 325–344.
- Oberg, A. L., and D. W. Mahoney. 2007. "Linear Mixed Effects Models." In *Topics in Biostatistics*, edited by W. T. Ambrosius, 213–234. Totowa, New Jersey: Humana Press .
- Pádua, L., N. Guimarães, T. Adão, P. Marques, E. Peres, A. Sousa, and J. J. Sousa. 2019. "Classification of an Agrosilvopastoral System Using RGB Imagery from an Unmanned Aerial Vehicle." In *Progress in Artificial Intelligence*. EPIA 2019.

- Lecture Notes in Computer Science*, edited by R. Goebel, Y. Tanaka, W. Wahlster, and J. Siekmann, 248–257. Vol. 11804. Cham, Switzerland: Springer. doi:10.1007/978-3-030-30241-2_22.
- Pauli, H., M. Gottfried, A. Lamprecht, S. Niessner, S. Rumpf, M. Winkler, K. Steinbauer, and G. Grabherr. 2015. *The GLORIA Field Manual – Standard Multi-Summit Approach, Supplementary Methods and Extra Approaches*. 5th ed. Vienna: Global Observation Research Initiative in Alpine Environments (GLORIA), Austrian Academy of Sciences & University of Natural Resources and Life Sciences Vienna, Austria. doi:10.2777/095439.
- Pedregosa, F., G. Varoquaux, A. Gramfort, V. Michel, B. Thirion, O. Grisel, M. Blondel, et al. 2011. “Scikit-Learn: Machine Learning in Python.” *Journal of Machine Learning Research* 12:2825–2830. doi:10.1007/s13398-014-0173-7.2.
- Peel, M. C., B. L. Finlayson, and T. A. McMahon. 2007. “Updated World Map of the Köppen-Geiger Climate Classification.” *Hydrology and Earth System Sciences Discussions* 4 (2): 439–473.
- Pierrot-Deseilligny, M. 2016. *MicMac, Apero, Pastis and Other Beverages in a Nutshell*. <http://logiciels.ign.fr/?Telechargement,20>.
- Piewak, F., P. Pinggera, M. Enzweiler, D. Pfeiffer, and Z. Marius. 2018. “Improved Semantic Stixels via Multimodal Sensor Fusion,” September. <http://arxiv.org/abs/1809.08993>.
- Pirotti, F., A. Guarnieri, and A. Vettore. 2013. “State of the Art of Ground and Aerial Laser Scanning Technologies for High-Resolution Topography of the Earth Surface.” *European Journal of Remote Sensing* 46 (1): 66–78. doi:10.5721/EuJRS20134605.
- Pirotti, F., and F. Tonion. 2019. “Classification of Aerial Laser Scanning Point Clouds Using Machine Learning: A Comparison between Random Forest and Tensorflow.” *International Archives of the Photogrammetry, Remote Sensing and Spatial Information Sciences - ISPRS Archives* 42 (2/W13): 1105–1111. doi:10.5194/isprs-archives-XLII-2-W13-1105-2019.
- R Core Team. 2018. “R: A Language and Environment for Statistical Computing.” Vienna, Austria: R Foundation for Statistical Computing. <https://www.r-project.org/>.
- Räsänen, A., and T. Virtanen. 2019. “Data and Resolution Requirements in Mapping Vegetation in Spatially Heterogeneous Landscapes.” *Remote Sensing of Environment* 230 (April): 111207. Elsevier. doi:10.1016/j.rse.2019.05.026.
- Rieg, L., V. Wichmann, M. Rutzinger, R. Sailer, T. Geist, and J. Stter. 2014. “Data Infrastructure for Multitemporal Airborne LiDAR Point Cloud Analysis - Examples from Physical Geography in High Mountain Environments.” *Computers, Environment and Urban Systems* 45: 137–146. Elsevier Ltd. doi:10.1016/j.compenvurbsys.2013.11.004.
- Rieke-Zapp, D. H., R. Rosenbauer, and F. Schlunegger. 2009. “A Photogrammetric Surveying Method for Field Applications.” *The Photogrammetric Record* 24 (125): 5–22. doi:10.1111/j.1477-9730.2008.00515.x.
- Silván-Cárdenas, J. L., and L. Wang. 2006. “A Multi-Resolution Approach for Filtering LiDAR Altimetry Data.” *ISPRS Journal of Photogrammetry and Remote Sensing* 61 (1): 11–22. doi:10.1016/j.isprsjprs.2006.06.002.
- Smith, M. W., J. L. Carrivick, and D. J. Quincey. 2015. “Structure from Motion Photogrammetry in Physical Geography.” *Progress in Physical Geography* 40 (2): 247–275. doi:10.1177/0309133315615805.
- Smith, M. W., J. L. Carrivick, and D. J. Quincey. 2016. “Structure from Motion Photogrammetry in Physical Geography.” *Progress in Physical Geography: Earth and Environment* 40 (2): 247–275. doi:10.1177/0309133315615805.
- Tsai, V. J. D. 2006. “A Comparative Study on Shadow Compensation of Color Aerial Images in Invariant Color Models.” *IEEE Transactions on Geoscience and Remote Sensing* 44 (6): 1661–1671. doi:10.1109/TGRS.2006.869980.
- Wagner, W., C. Eberhöfer, M. Hollaus, and G. Summer. 2004. “Robust Filtering of Airborne Laser Scanner Data for Vegetation Analysis.” *International Archives of Photogrammetry, Remote Sensing and Spatial Information Sciences* XXXVI (8/W2): 56–61.
- Wakulińska, M., and A. Marcinkowska-Ochtyra. 2020. “Multi-Temporal Sentinel-2 Data in Classification of Mountain Vegetation.” *Remote Sensing* 12 (17): 2696. doi:10.3390/rs12172696.
- Wallace, L., D. S. Saldias, K. Reinke, S. Hillman, B. Hally, and S. Jones. 2019. “Using Orthoimages Generated from Oblique Terrestrial Photography to Estimate and Monitor Vegetation Cover.” *Ecological Indicators* 101 (February 2018): 91–101. Elsevier. doi:10.1016/j.ecolind.2018.12.044.
- Wehr, A., and U. Lohr. 1999. “Airborne Laser Scanning—an Introduction and Overview.” *ISPRS Journal of Photogrammetry and Remote Sensing* 54 (2–3): 68–82. doi:10.1016/S0924-2716(99)00011-8.
- Westoby, M. J., J. Brasington, N. F. Glasser, M. J. Hambrey, and J. M. Reynolds. 2012. “‘Structure-from-motion’ Photogrammetry: A Low-Cost, Effective Tool for Geoscience Applications.” *Geomorphology* 179: 300–314. Elsevier B.V. doi:10.1016/j.geomorph.2012.08.021.
- Winkler, M., A. Lamprecht, K. Steinbauer, K. Hülber, J.-P. Theurillat, F. Breiner, P. Choler, et al. 2016. “The Rich Sides of Mountain Summits – A Pan-European View on Aspect Preferences of Alpine Plants.” *Journal of Biogeography* 43 (September): 2261–2273.
- Wobbecke, D. M., G. Meyer, K. Von Bargaen, and D. Mortensen. 1995. “Color Indices for Weed Identification under Various Soil, Residue, and Lighting Conditions.” *Transactions of the ASAE* 38: 259–269.
- Zellweger, F., P. De Frenne, J. Lenoir, D. Rocchini, and D. Coomes. 2019. “Advances in Microclimate Ecology Arising from Remote Sensing.” *Trends in Ecology and Evolution* 34 (4): 327–341. Elsevier Ltd. doi:10.1016/j.tree.2018.12.012.
- Zhang, J., Y. Yao, and N. Suo. 2020. “Automatic Classification of Fine-Scale Mountain Vegetation Based on Mountain Altitudinal Belt.” *Plos One* 15 (8):

e0238165. Edited by Julian Aherne. doi:[10.1371/journal.pone.0238165](https://doi.org/10.1371/journal.pone.0238165).

Zuur, A. F., E. N. Ieno, N. Walker, A. A. Saveliev, and G. M. Smith. 2009. *Mixed Effects Models and Extensions in Ecology with*

R. Statistics for Biology and Health, edited by M. Gail, K. Krickeberg, J. M. Samet, A. Tsiatis, and W. Wong. New York: Springer New York. doi:[10.1007/978-0-387-87458-6](https://doi.org/10.1007/978-0-387-87458-6).